EBioMedicine 30 (2018) 129–137

Contents lists available at ScienceDirect

EBioMedicine

journal homepage: www.ebiomedicine.com

Research Paper

Plectin-1 Targeted Dual-modality Nanoparticles for Pancreatic Cancer Imaging

Xiao Chen [a,b,1], Hao Zhou [a,1], Xiaoshuang Li [a], Na Duan [a], Shouyou Hu [c], Yongkang Liu [a], Yali Yue [a], Lina Song [a], Yifen Zhang [d], Donghui Li [e], Zhongqiu Wang [a,*]

[a] Department of Radiology, Affiliated Hospital of Nanjing University of Chinese Medicine, Nanjing 210029, China
[b] Division of Nephrology, Zhongshan Hospital Fudan University, Shanghai 200032, China
[c] Department of Oncology, Affiliated Hospital of Nanjing University of Chinese Medicine, Nanjing 210029, China
[d] Department of Pathology, Affiliated Hospital of Nanjing University of Chinese Medicine, Nanjing 210029, China
[e] Department of Gastrointestinal Medical Oncology, The University of Texas MD Anderson Cancer Center, Houston, TX 77030, USA

ARTICLE INFO

Article history:
Received 16 January 2018
Received in revised form 9 March 2018
Accepted 9 March 2018
Available online 15 March 2018

Keywords:
Pancreatic cancer
Plectin-1
Magnetic resonance imaging
Optical imaging
Nanoparticle

ABSTRACT

Background: Biomarker-targeted molecular imaging holds promise for early detection of pancreatic cancer. The aim of this study was to design and evaluate a plectin-1 targeted multi-functional nanoparticle probe for pancreatic cancer imaging.

Methods: 1,2-Distearoyl-sn-glycero-3-phosphoethanolamine-N-amino(polyethylene glycol) (DSPE-PEG-NH2)-modified superparamagnetic iron oxide (Fe_3O_4) nanoparticles (SPION) were conjugated with plectin-1 antibody and/or Cy7 to create the multi-functional targeted nanoparticle targeted probe (Plectin-SPION-Cy7) or non-targeted probe (SPION-Cy7). Pancreatic carcinoma cell lines expressing plectin-1 were cultured with the targeted or control probes and then were imaged using confocal laser scanning microscopy and magnetic resonance imaging (MRI). Accumulations of the nanoparticles in pancreatic tumor xenografted mice were determined by MRI and fluorescence imaging.

Results: *In vitro* optical imaging and MRI showed that the targeted nanoparticles were highly accumulated in MIAPaCa2 and XPA-1 carcinoma cells but not in non-carcinoma MIN6 cells, which was further confirmed by Prussian blue staining. *In vivo* MRI showed a significant T2 signal reduction. Prussian blue staining further confirmed that the plectin-1 targeted nanoparticles were highly accumulated in the tumor mass but not in normal pancreatic tissues, or in the liver and kidney, and few nanoparticles were observed in the tumors of mice injected with SPION-Cy7.

Conclusions: Our data demonstrate that plectin-1 targeted fluorescence and MR dual-functional nanoparticle can visualize pancreatic cancer, and it has great potential to be used with various imaging devices for pancreatic cancer detection.

1. Introduction

Pancreatic cancer is a highly aggressive and rapidly fatal malignancy with a 5-year survival rate of <5% (Jemal et al., 2008). Surgical resection of the tumor is the only possible cure but most patients are usually diagnosed with unresectable late stage disease (Willett et al., 2005). Therefore, the prognosis is poor. Early detection at the potentially curable stage is critical to reduce the mortality of pancreatic cancer. However, conventional imaging technology, such as ultrasonography, computed tomography (CT), and magnetic resonance imaging (MRI) have not significantly increased our ability to detect early-stage disease or affect outcomes of pancreatic cancer patients (Cote et al., 2013). In addition, conventional imaging is limited in differentiating malignancy from benign lesions. Thus, overtreatment of patients with pancreatic benign cystic lesions could occur. Therefore, there is an unmet clinical need to develop agents for early detection. Endoscopic imaging and molecular-based radiographic tests hold the promise to help precisely identify pancreatic malignant lesions and their precursors at early stages. Furthermore, molecular imaging could improve our understanding of disease pathogenesis and identify diagnostic markers and therapeutic targets.

Recently, targeted molecular imaging has shown an advantage in early detection of cancer with high specificity and sensitivity in animal models (Weissleder, 2006). Optical imaging (fluorescence and bioluminescence), MR imaging, ultrasound, and positron emission tomography have been developed for *in vivo* molecular imaging (Massoud and

* Correspondence author.
E-mail address: zhq2001us@163.com (Z. Wang).
[1] Xiao Chen and Hao Zhou contributed equally to this work.

https://doi.org/10.1016/j.ebiom.2018.03.008

Gambhir, 2003). Fluorescence imaging is usually used for its low costs of detection devices, easy use and interpretation, and absence of ionizing radiation (Ntziachristos, 2010). Near-infrared (NIR) imaging has the advantage of improved tissue penetration (up to 1 cm) and low tissue auto-fluorescence (Weissleder and Ntziachristos, 2003; Weissleder, 2006; Houghton et al., 2015). Magnetic nanoparticles (MNPs) can induce changes in T2-or T2*-weight MR images and have been considered as good carriers for targeted molecules with high biocompatibility and low toxicity (Vuong et al., 2012). Optical imaging and/or MR imaging has been applied for pancreatic cancer imaging in previous studies (Yang et al., 2009; Tong et al., 2013; Wang et al., 2016).

Targeted molecules are crucial in the design of molecular imaging probes. Targeted molecules should be highly expressed in cancer cells but absent or under-expressed in normal adjacent tissues (Yang et al., 2009). To find such target molecules, CA19.9 (Houghton et al., 2015), urokinase plasminogen activator (Yang et al., 2009), claudin-4 (Neesse et al., 2013), surviving(Tong et al., 2013; Wang et al., 2016), insulin-like growth factor-1 receptor (IGF-1R) (Park et al., 2016; England et al., 2016), integrin αvβ6 (Liu et al., 2014), integrin αvβ3 (Trajkovic-Arsic et al., 2014) and galectin-1 (Rosenberger et al., 2015) have been tested in pancreatic cancer imaging. Kelly et al. (2008) first identified that plectin-1 is highly expressed in invasive pancreatic cancer. Bausch et al. (2011) further showed that 93% of pancreatic ductal adenocarcinoma cases are plectin-1 positive, and the specificity and sensitivity of plectin-1 in distinguishing malignant from benign lesions are 83% and 84%, respectively. Konkalmatt et al. (2013) further showed that plectin-1 peptide targeted adeno-associated virus (AAV) vector could be selectively delivered to pancreatic carcinoma cells *in vivo*, which suggests applicability for early detection and treatment of pancreatic cancer. Wang et al. (2014) also showed that plectin-1 targeted dye bovine serum albumin (BSA)·superparamagnetic iron oxide nanoparticles (SPION)- monoclonal antibody (mAb) bioconjugates, but not the non-targeted bioconjugates could bind to the Panc-1 cells. Findings of these studies suggest that plectin-1 has the potential to be a molecular target for pancreatic cancer imaging. However, Konkalmatt et al. (2013) used AAV targeting peptide as the target molecule, and they only showed the optical imaging. Kelly et al. (2008) also used plectin-1 targeting peptide and only showed the MRI data of agar-embedded specimen. Wang et al. (2014) used the BSA-modified nanoparticles and only showed the efficiency of the probe in *in vitro* study. Further studies are required due to the limited number of imaging investigations using plectin-1 as a target.

In the present study, we designed a fluorescence and MR dual-modality magnetic nanoprobe targeting plectin-1 and evaluated its ability for pancreatic cancer imaging in both *in vitro* and *in vivo* experiments.

2. Materials and Methods

2.1. Detection of Plectin-1 Expression in Cell Lines

Plectin-1 protein expressions in four pancreatic cancer cell lines, MIAPaCa2, Panc-1, BxPC-3, XPA-1 and one pancreatic beta cell line MIN6 were determined using Western blot. Briefly, cellular protein was obtained using radioimmunoprecipitation assay (RIPA) lysis buffer. Thirty microgram of proteins was separated on a 7% Bis-Tris NuPAGE gel (Invitrogen) for 3 to 4 h at 60 v and blotted onto polyvinylidene difluoride (PVDF) membranes. The PVDF membrane was blocked with 5% (w/v) skim milk for 1 h at room temperature and then incubated with an anti-plectin-1 primary monoclonal antibody diluted as recommended by the manufacturer (Abcam, Cat# ab32528, MA, USA) at 4 °C overnight. The membrane was washed in TBST for three times, and then incubated with a secondary antibody conjugated with horseradish peroxidase at room temperature for 1 h. After washing, the bands were visualized using enhanced chemiluminescence. β-Actin was used as a loading control. Two independent experiments were performed.

2.2. Design and Synthesis of Plectin-SPION-Cy7 (Cyanine 7)

1,2-Distearoyl-sn-glycero-3-phosphoethanolamine-N-amino(polyethylene glycol) was dispersed in chloroform and mixed with the superparamagnetic iron oxide (Fe_3O_4) nanoparticles (obtained as a general gift from Southeast University, Nanjing China) and deionized water. The mixture was then rotated and evaporated at 65 °C for 13 min to obtain NH2-PEG-SPIONs (NP-SPION). The oil-dispersible iron oxide nanoparticles can be modified with amphiphilic polymers by the hydrophobic interaction. The hydrophobic ligand of SPIONs binds with the hydrophobic end of amphiphilic polymers by the hydrophobic interaction. The hydrophilic group at the outer surface made the NP-SPION soluble. The solution was centrifuged (3000 rpm/min) for 5 min and dispersed in deionized water by using ultrasonic oscillation. The mixture was filtrated with a 0.22 μm filter several times before storage. The synthesized NP-SPION was mixed with 2-(N-Morpholino) ethanesulfonic acid buffer, and then carbodiimide hydrochloride (EDC) and sulfo- N-hydroxysulfosuccinimide (NHS) solutions. The mixture was shaken in a swing bed (150 rpm) for 30 min, centrifuged at 3000 rpm/min for 3 min, and then washed twice with borate buffer. Then, 20 μg of anti-plectin-1 monoclonal antibody (0.5 mg/ml, Abcam, MA, USA) and/or 700 μg of Cy7 NHS (Near infrared fluorescent, NIRF; Sigma-Aldrich, MO, USA) were added to get Plectin-SPION-Cy7 or SPION-Cy7. The Plectin-SPION-Cy7 was purified by gel chromatography. For SPION-Cy7, the unbound Cy7 was removed by centrifugation. The final solution was shaken in a swing bed for 12 h, and then stored away from light at 4 °C.

2.3. Characterizations of the Targeted Probe

The size of the targeted magnetic probe was determined using a transmission electron microscope (Joel, JEM-200CX, Japan). Briefly, the samples were dispersed in alcohol (25 μg Fe/ml), then deposited onto the double copper grids, carbon coated (Electron Microscopy Sciences, PA, USA) and left until the excess liquid volatilized, and then were dried under infrared light. Samples were imaged at an acceleration voltage of 180 kV. Then, the samples were diluted with deionized water. The hydrodynamic sizes and zeta potential of SPION, SPION-Cy7, and Plectin-SPION-Cy7 were measured using a Zetasizer (Beckman, Delsa 440SX, Germany) at pH of 7.0–7.2. The relaxivity values of r1 and r2 were calculated by fitting the 1/T1 and 1/T2 relaxation time (s^{-1}) *versus* Fe^{3+} concentration (mM) curves by using an NMR Analyzer(Bruker Optik GmbH, Ettlingen, Germany). The T2-weighted images were acquired using a T2-weighted spin echo pulse sequence with TR = 1200 ms, TE = 110 ms, field of view (FOV) = 100 × 120 mm^2, data matrix = 280 × 216, slice thickness = 2 mm by using 1.5 T MRI (AChieva 1.5 T, Philips, the Netherland). The precipitated solid was dried at 40 °C after washing three times. Magnetic properties were analyzed using vibrating sample magnetometry (VSM, Lakeshore 7407, USA) with a saturating field of 1.0 Tesla. The stability of SPION in sodium chloride (0 to 1.0 mM) solution (contain 5% BSA) and in the solutions of varying pH values (3 to 11) were also observed for 7 days. In addition, we analyzed the particle size and polydispersity index (PDI) *via* dynamic light scattering (DLS) using a Zetasizer at 1st and 7th days in phosphate-buffered saline (PBS) and 20% serum solution. The results are expressed as mean ± standard deviation ($n = 3$). Two independent characterizations were performed.

2.4. In Vitro Optical and MRI Imaging and Prussian Blue Staining

The MIAPaCa2, XPA-1 and MIN6 cells (1.0×10^5 cells/well) were plated in 6-well plates and cultured in Iscove's Modified Dulbecco's Medium (IMDM) or Dulbecco's modified Eagle's medium (DMEM) containing 10% fetal bovine serum (FBS; Sigma, USA), 100 U/ml penicillin and 100 μg/ml streptomycin at 37 °C in a humidified atmosphere of 95% air and 5% CO_2 with medium change every 2 days. Upon reaching 50–60%

confluences, SPION-Cy7 and Plectin-SPION-Cy7 were added, and the cells were cultured for 24 h. Control cells did not receive any nanoparticles. The harvested cells were washed 3 times with PBS and fixed in 4% polyoxymethylene, stained using Hoechst Kit according to the manufacturer's instruction (Hoechst at 5 μg/ml), and then imaged using the confocal laser scanning microscope (Nikon C2 Plus, Japan). Part of the cells was fixed as described above for Prussian blue staining (1:1 mixture of 1 mol/l hydrochloric acid and potassium ferrocyanide). For MRI, the cells were harvested, washed, and resuspended in 1% agarose. T2 relaxation times were calculated using a T2-multi-echos pulse sequence with TR = 3000 ms, TE = 22–352 ms (16TE), FOV = 100× 120 mm^2, data matrix = 280 × 216, slice thickness = 5 mm, slice gap = 1 mm. We also investigated the association between plectin-1 expression and fluorescent signal (Image J) or T2 relaxation times. Three independent experiments were performed.

2.5. Pharmacokinetic Study

The pharmacokinetic behavior of SPION-Cy7 and Plectin-SPION-Cy7 were evaluated as follows. Eight-week-old nude mice weighing 21–24 g were kept in specific pathogen-free facilities (21 ± 1 °C, 50–80% relative humidity; a 12 h light-12 h dark cycle) and randomly divided into 2 groups (n = 3). They had access to water and feed freely. The two types of nanoparticles (at the dose of 100 μg Fe) were intravenously injected *via* tail vein. Blood (200 μl) were collected at 0.2 h, 1 h, 4 h, 8 h, 12 h, 24 h, 48 h and 72 h post-injection, respectively. The nanoparticles in serum samples were quantified by measuring the concentration of Fe with inductively coupled plasma mass spectrometry (ICP-MS, NexION 350, PerkinElmer, USA). The basic levels of Fe were also measured. The Fe concentration-time profile was plotted. The following parameters, half-life ($T_{½}$), clearance, and area under the curve (AUC) from 0 to t (AUC_{0-t}) were calculated using PKSolver. Two independent experiments were performed. All experiments were carried out according to the National Institutes of Health guide for the Care and Use of Laboratory animals (NIH Publications No. 8023, revised 1978) and were approved by the Animal Use Committee of the Affiliated Hospital of Nanjing University of Chinese Medicine.

2.6. Orthotropic Human Pancreatic Tumor Xenograft Model

The pancreatic tumor xenograft model was established as previously described (Wang et al., 2016). Briefly, twenty-seven 8-week-old nude mice weighing 20–25 g were kept in specific pathogen-free facilities and maintained under conventional conditions (21 ± 1 °C, 50–80% relative humidity) in a 12 h light-12 h dark cycle. They had access to water and feed freely. Approximately 5 × 10^6 of red fluorescent protein (RFP)-expressing XPA-1 cells (AntiCancer Inc., San Diego, USA) were subcutaneously injected into the flank of three mice. Three weeks later, tumors were resected aseptically when the tumor grew to 1.0 cm in diameter. Then the solid tumor tissues were cut into 1.0 × 1.0 × 1.0 mm sections and surgically transplanted into the pancreas of 24 mice. A fluorescence stereo microscope model MZ650 (Nanjing Optic Instrument Inc. China) equipped with D510 long-pass and HQ600/50 band-pass emission filters (Chroma Technology, Brattleboro, VT, USA) with a cooled colour charge-coupled device camera (Qimaging, BC, Canada) was used to monitor the tumor growth. When the tumors reached to 5 to 10 mm in diameter, they were suitable for MR targeted imaging. They were randomly divided into six groups (n = 4). All experiments were carried out according to the National Institutes of Health Guide for the Care and Use of Laboratory animals (NIH Publications No. 8023, revised 1978) and were approved by the Animal Use Committee of the Affiliated Hospital of Nanjing University of Chinese Medicine.

2.7. In Vivo MR Imaging

Scanning of tumor-bearing mice was performed on a 3.0 Tesla MR scanner (Siemens Magnetom Trio Tim, Germany) using an animal coil as described in our previous study (Wang et al., 2016). Briefly, mice were anesthetized using ketamine (4.0 mg/100 g), and were scanned prior to, and 8 h, 24 h and 48 h after injection with the SPION-Cy7 (n = 12) or Plectin-SPION-Cy7 (n = 12) probes through the tail vein. T1- and T2-weighted imaging were performed: TR of 1040 ms and TE of 14 ms were used for T1WI and TR of 4000 ms and TE of 75 ms were used for T2-weighted fast spin echo imaging, a FOV of 52 mm × 52 mm, slice thickness of 1 mm with a 0.1 mm slice gap. The imaging sequences of the multi-T2 map were described as follows: TR/TE 2000 ms/8.0–110 ms (8 TE), contrast 12, slices with 1.5 mm. T2 values of each tumor in mice were obtained from T2 map at the Siemens Syngo workplace.

2.8. In Vivo Optical Imaging

After MR imaging, optical imaging was performed using the IVIS Spectrum pre-clinical *in vivo* imaging system (PerkinElmer, MA, USA). A 590-nm excitation and 610-nm emission filter set with a 40-s exposure time were adopted for tumor detection (red fluorescence). For the detection of Plectin-SPION-Cy7, A 750 nm excitation and 773 nm emission filter set with a 60-s exposure time were adopted. Then the two images detected by different fluorescence methods were overlaid, and the overlapping images indicated the distribution of the targeted nanoparticles in the tumor.

2.9. Histological Examination

Tumors and normal adjacent tissues of the pancreas as well as normal tissues of the liver, spleen, and kidney were collected, fixed in formaldehyde solution at 4 °C for 24 h, and embedded in paraffin. Tissue sections were stained with hematoxylin and eosin (H&E) or Prussian blue solution. Prussian blue positive cells per high magnification field (×100) of vision were counted. Five fields with the maximum blue-positive cells were counted in each image.

2.10. Statistical Analysis

SPSS 16.0 (SPSS Inc., Chicago, USA) was applied for data management and statistical analysis. Data are expressed as mean ± standard deviation (SD) and analyzed by one-way analysis of variance (ANOVA), where P values below 0.05 were considered as statistically significant.

3. Results

3.1. Plectin-1 Protein Expression

Western blot shows that plectin-1 is expressed in pancreatic carcinoma cell lines MIAPaCa2, BxPC-3, Panc-1, and XPA-1 (Fig. 1), but the expression level was very low in MIN6 beta cells. MIAPaCa2 and XPA-1 cells, which had the highest and moderate levels of plectin-1 expression, were used in later experiments. Similar trends were observed in the two independent detections.

3.2. Characterization of the Targeted Magnetic Probe

The characteristics of the targeted magnetic probe are shown in Fig. 2. The SPION has a core size of 12 nm (9-15 nm, Fig. 2B). The sizes of SPION-Cy7 and Plectin-SPION-Cy7 are shown in Fig. 2C. The T2WI signals of SPION decreased in a dose-dependent manner (Fig. 2D). The SPIONs had a short T2 relaxation time and high r2/r1 ratio with an r2 value of 116.0 mM^{-1} s^{-1} and r1 values of 7.6 mM^{-1} s^{-1} (Fig. 2D).

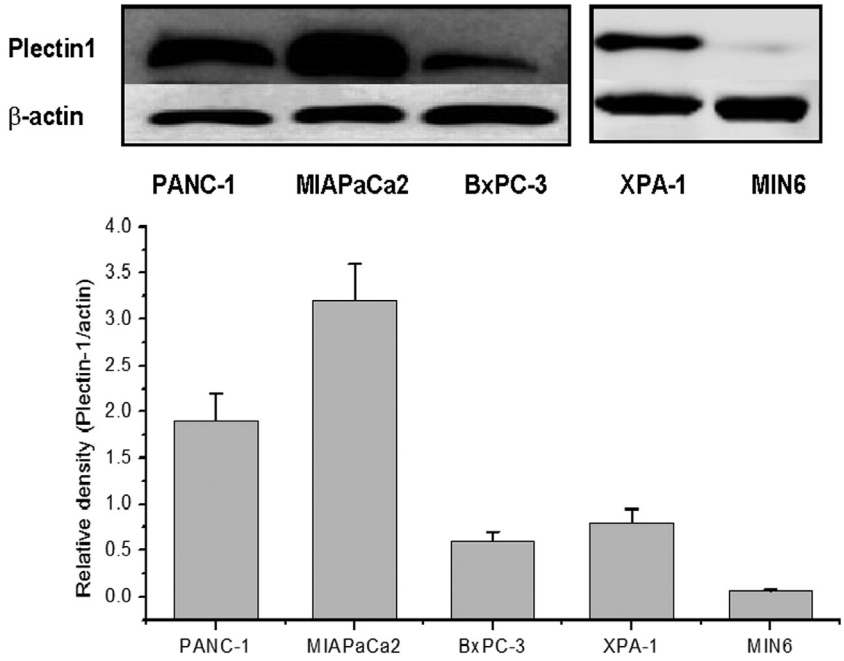

Fig. 1. Plectin-1 expression in four pancreatic cancer cell lines (MIA PaCa2, BxPC-3, Panc-1, XPA-1) as detected by Western blot. MIA PaCa2 and Panc-1 show higher expression levels than BxPC-3 and XPA-1 cells. Very low level of expression is observed in normal pancreatic beta cell line MIN6.

The hysteresis curve of VSM shown in Fig. 2E demonstrates that SPION have good superparamagnetism property. The diameter of hydrodynamic size of SPION, SPION-Cy7 and Plectin-SPION-Cy7 were 28.9 ± 3.8 nm, 55.8 ± 10.4 nm and 84.3 ± 15.3 nm, respectively (Fig. 2F). The potentials of SPION, SPION-Cy7 and Plectin-SPION-Cy7 were 15.9 ± 5.3 mV, −24.8 ± 6.2 mV and −11.3 ± 5.6 mV, respectively (Fig. 2G). No significant differences were observed in the hydrodynamic size and PDI of Plectin-SPION-Cy7 at 1 and 7 days in PBS and 20% serum solution (Fig. 2H) and no obvious deposition was observed in NP-SPION solution (Supplemental Fig. 1), which indicates that the NH_2-PEG·SPION was stable. We also determined the Fourier transform infrared (FTIR) features of NH_2-PEG and NH_2-PEG-SPIONs (NP-SPION) as shown in Supplementary Fig. 2. Similar results were observed in the two independent detections.

3.3. The Specific Accumulation of Targeted Nanoparticles In Vitro

The accumulations of Plectin-SPION-Cy7 in pancreatic cancer cells and normal MIN6 cells were detected as a red fluorescent signal by optical imaging. No obvious fluorescent signals were detected in MIN6 cells after 20 h of culture with SPION-Cy7 or Plectin-SPION-Cy7 (Fig. 3). A weaker fluorescent signal was detected in MIAPaCa2 and XPA-1 cells cultured with SPION-Cy7. A stronger red fluorescent signal was observed in the membrane and cytoplasm of MIAPaCa2 and XPA-1 cells cultured with Plectin-SPION-Cy7 (Fig. 3). Plectin-1 expression was positively correlated with the fluorescent signal ($r = 0.91$, $p < 0.01$) (Supplemental Fig. 3). Similar results were observed in the two independent detections.

The accumulation of Plectin-SPION-Cy7 in carcinoma cells was also confirmed by MR imaging and Prussian blue staining. The reduction of T2 values (deltaT2) in MIAPaCa2 and XPA-1 cells cultured with Plectin-SPION-Cy7 was significantly ($p < 0.01$) higher than those cultured with SPION–Cy7 (19.2 ± 6.3 *vs.* 6.0 ± 2.6 ms and 9.6 ± 3.8 *vs.* 2.2 ± 3.3 ms, respectively) (Fig. 4B). In addition, the deltaT2 in MIAPaCa2 was higher than that of XPA-1($p < 0.05$, Fig. 4B), and the T2 signal in MIAPaCa2 was lower than that of XPA-1, which indicated that the accumulation of Plectin-SPION-Cy7 was correlated with the plectin-1 expression ($r = -0.87$. $p < 0.01$) (Supplemental Fig. 3). Similar results were observed in the two independent detections. The control cells that were not exposed to the probes had the values of 38.0 ± 13.2 ms, 36.3 ± 9.4 ms, and 40.2 ± 11.2 ms. No obvious difference in T2 signal was observed in MIN6 cells cultured with SPION-Cy7 or Plectin-SPION-Cy7 (29.8 ± 8.6 *vs* 32.3 ± 10.7 ms). The frequency of iron positive cells in the carcinoma cell lines were higher than that in MIN6 cells when cells were cultured with Plectin-SPION-Cy7 (Fig. 5). In addition, the number of positive iron staining cells in the carcinoma cell lines was greater in cells incubated with Plectin-SPION-Cy7 than those incubated with SPION-Cy7 (Fig. 5).

3.4. The Specific Accumulation of Targeted Nanoparticles in Pancreatic Tumors

The half-life (t1/2), clearance and AUC_{0-t} were 18.9 ± 3.3 h, 0.20 ± 0.14 ml/h, and 448.61 ± 36.7 μg/ml* h for Plectin- SPION-Cy7, and were 13.6 ± 2.4 h, 0.34 ± 0.13 ml/h and 276.46 ± 23.4 μg/ml* h for SPION-Cy7 in nude mice. The concentration-time curves are shown in Supplemental Fig. 4.

Fig. 6 shows the MR imaging of tumors pre- or post-injection of Plectin- SPION-Cy7 or SPION-Cy7. Both T2WI (Fig. 6A) and T2 maps (Fig. 6B) showed that the T2 signal was decreased in pancreatic tumors 48 h after injection with Plectin-SPION-Cy7 compared to the pre-injection signal. However, no significant T2 signal decrease was found at 8 h and 24 h after Plectin-SPION-Cy7 injection. On the contrary, no significant changes of T2 signal were detected in tumor-bearing mice administered with SPION-Cy7 (Fig. 6C and D), which indicated that Plectin-SPION-Cy7 was preferentially accumulated in the tumor tissues. Quantitative analysis showed that the T2 values in mice administered with Plectin-SPION-Cy7 at 48 h was significantly lower than that at pre-contrast (0 h) or that in mice receiving SPION-Cy7 (Fig. 6E, $p < 0.001$ and $p < 0.05$, respectively). T2 values at 48 h after Plectin-SPION-Cy7 injection was also significantly lower than that at 8 h and 24 h (Fig. 6E, $p < 0.05$). In addition, T2 signals in the liver (Fig. 6F) and spleen (Fig. 6G), but not in the kidney, were also decreased after injection with Plectin-SPION-Cy7 (7H). Optical imaging showed that in SPION-Cy7 administered tumor-bearing mice, the near infrared fluorescent (NIRF) signals were mainly detected in the spleen, not in the tumors at 8 h, 24 h and 48 h and in mice administered with Plectin-

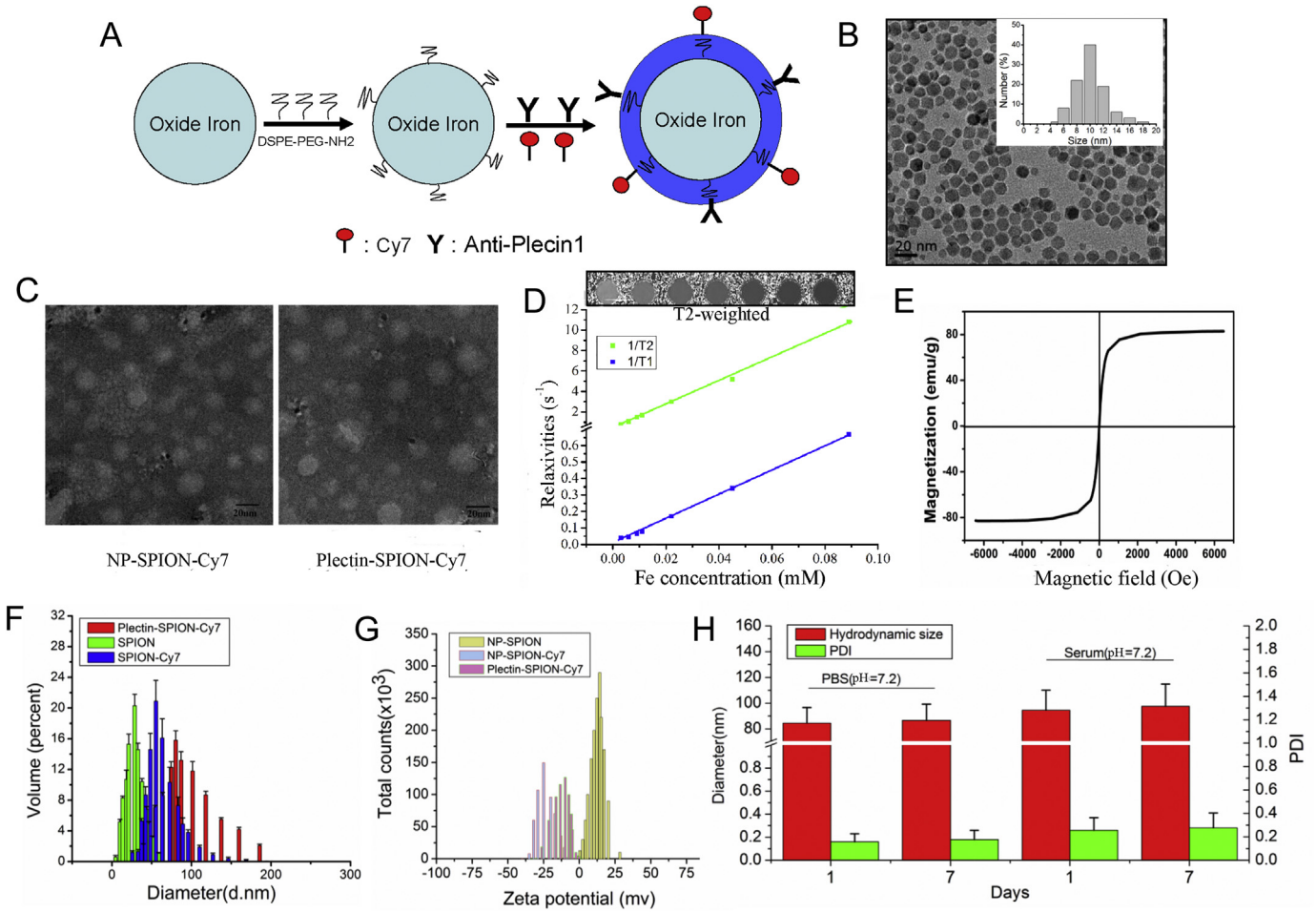

Fig. 2. Characterization of molecular probe. (A) The schematic representation of plectin-1 targeted fluorescent (Cy7) and MR (SPION) nanoprobe (Plectin-SPION-Cy7). (B) The size of nanoparticles. The DSPE-PEG-NH2-modified SPION (NP-SPION) has a core size of 12 nm. (C) The size of SPION-Cy7 and Plectin-SPION-Cy7 under transmission electron microscope. (D) SPION shortens T_2 relaxation time with an r_2 value of 116.0 mM^{-1} s^{-1} and r1 values of 7.6 mM^{-1} s^{-1}, which was examined at a 1.5 Tesla MR scanner. (D) The hysteresis curve demonstrates that SPION has good property of superparamagnetism. (E) The hydrodynamic sizes of SPION, SPION-Cy7 and Plectin-SPION-Cy7 are 28.9 ± 3.8 nm, 55.8 ± 10.4 nm and 84.3 ± 15.3 nm, respectively. (F) The zeta-potentials of SPION, SPION-Cy7 and Plectin-SPION-Cy7 are 15.9 ± 5.3 mV, −24.8 ± 6.2 mV and − 11.3 ± 5.6 mV, respectively. (G) No obvious changes in diameters and polydiversity index (PDI) are observed in Plectin-SPION-Cy7 solutions that were stored in phosphate-buffered saline (PBS) or serum at 4 °C for 7 days.

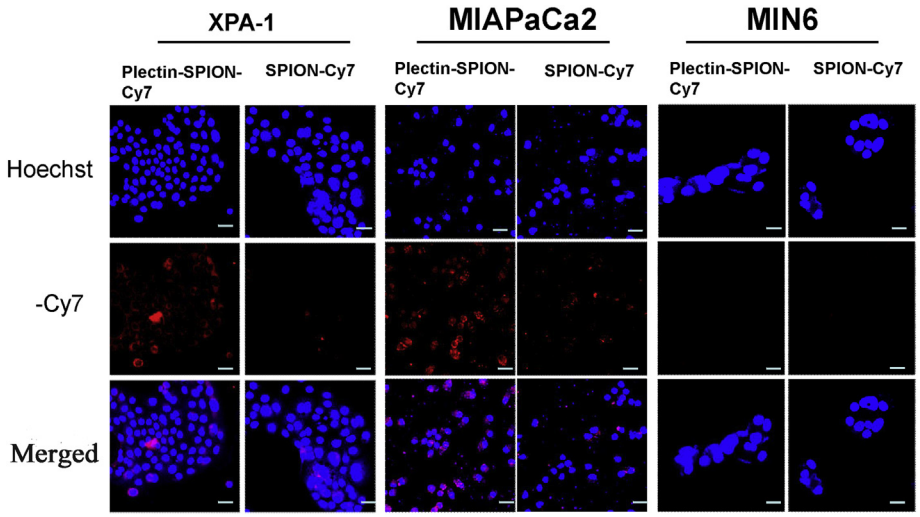

Fig. 3. Optical imaging of MIAPaCa2, XPA-1 and MIN6 cells cultured with medium containing SPION-Cy7 or Plectin-SPION-Cy7. Mild red fluorescence is detected in MIA PaCa2 and XPA-1 cells cultured with SPION-Cy7. A stronger red fluorescent signal is detected in the membrane and cytoplasm of MIAPaCa2 and XPA-1 cells cultured with Plectin-SPION-Cy7. No red fluorescence is observed in MIN6 cells cultured with SPION-Cy7 or Plectin-SPION-Cy7.

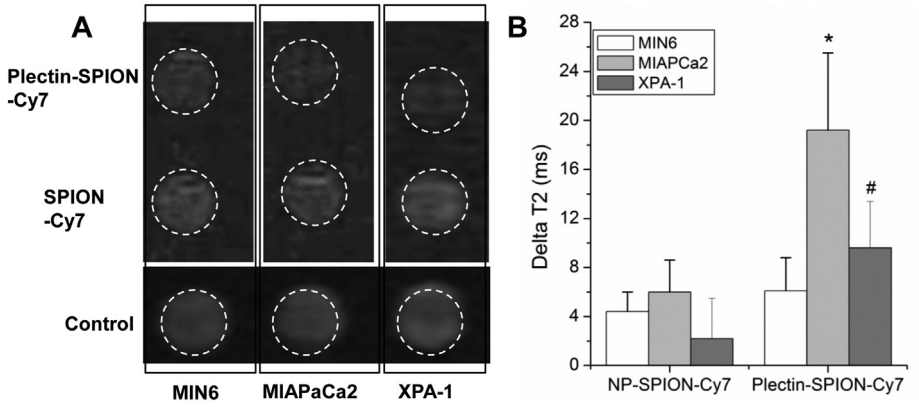

Fig. 4. SPION in MIAPaCa2, XPA-1 and MIN6 cells as detected by magnetic resonance imaging (MRI). Cells were cultured with medium containing SPION-Cy7 or Plectin-SPION-Cy7. The harvested cells were suspended in 1% agarose for MRI. Panel A shows decreased T2 signals in MIAPaCa2 and XPA-1 cells cultured with Plectin-SPION-Cy7 compared with that cultured with SPION-Cy7 or control. Panel B shows quantitative differences in delatT2 of MIAPaCa2 and XPA-1 cells but not MIN6 cells cultured with Plectin-SPION-Cy7 compared to those cultured with SPION-Cy7 or controls. In addition, the delatT2 of MIAPaCa2 is higher than XPA-1. $^{*}p < 0.01$ *vs* control or SPION-Cy7 within same cell lines;$\#p < 0.05$ *vs* control or SPION-Cy7 within same cell lines and MIAPaCa cultured with Plectin-SPION-Cy7.

SPION-Cy7, strong NIRF was detected in the pancreatic tumor at 48 h (Supplemental Fig. 5).

H&E staining and Prussian blue staining of the liver, kidney, spleen, normal pancreatic tissue, and pancreatic tumor are shown in Fig. 7. High levels of iron-positive cells were present in the spleen and pancreatic tumors, but few were observed in the liver, kidney and normal pancreatic tissues 48 h after injection of Plectin-SPION-Cy7 (Figs. 7 and 8). Iron-positive cells in the spleen and liver reached their peak at 24 h and then decreased at 48 h. In tumor-bearing mice administered SPION-Cy7, iron-positive cells were present in the liver and spleen, but few were observed in the pancreatic tumor, suggesting that Plectin-SPION-Cy7 was selectively accumulated in the tumor. At 48 h, there were far more iron-positive cells in the tumors of mice administered Plectin-SPION-Cy7 than in the tumors of the SPION-Cy7-treated group (Table 1). In addition, we examined the toxic effects of Plectin-SPION-Cy7 (0.25–1.0 mg/ml) on several organs by using histological methods. No tissue damage was observed. Only mild inflammation was observed (Supplemental Fig. 6).

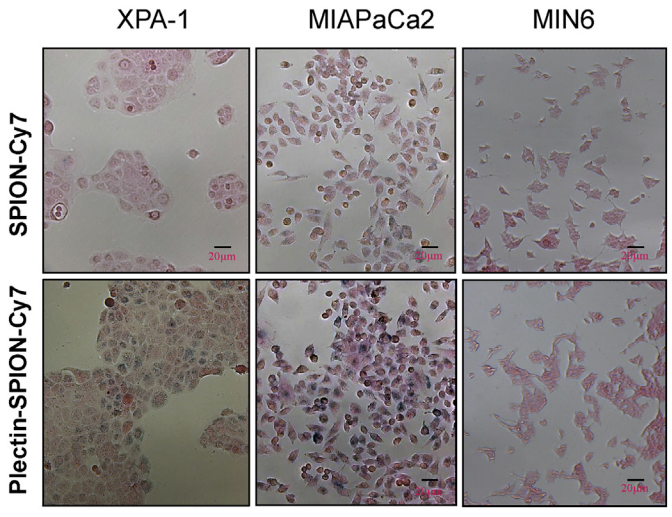

Fig. 5. SPION in MIAPaCa2, XPA-1 and MIN6 cells as detected by histological analysis. Prussian blue staining shows much more iron positive cells in cancer cells cultured with Plectin-SPION-Cy7 compare with that incubated with SPION-Cy7. Low number of iron positive cells and no difference is observed between the Plectin-SPION-Cy7 or SPION-Cy7 cultured MIN6 cells.

4. Discussion

Molecular imaging is an important approach for the early detection of cancer. In this study, we designed dual-functional plectin-1 targeted nanoparticles and demonstrated that these nanoparticles were specifically internalized by pancreatic cancer cells *in vitro* and selectively accumulated in orthotopic tumors *in vivo* using optical imaging and MRI approaches. Our findings suggest that plectin-1 targeted nanoparticles have a potential value for pancreatic cancer detection.

Traditional imaging technology such as CT and MRI often cannot detect pancreatic cancer at an early and potentially curable stage. The recent advances in molecular imaging offer a promising opportunity for early cancer detection, disease progression monitoring, and as well as targeted cancer therapy (Bogdanov et al., 2011; Kelly et al., 2008; Weissleder, 2006).

Identifying a tumor-specific biomarker is a critical step in molecular imaging. Among the many biomarkers that have been tested in molecular imaging of pancreatic cancer (Bergmann et al., 1995; Chen et al., 2007; Foygel et al., 2013; Lee et al., 2005; Nichols et al., 2004), plectin-1 has been recognized as an attractive target (Bausch et al., 2011; Kelly et al., 2008; Konkalmatt et al., 2013; Wang et al., 2014). Plectin-1 is a giant protein that links the three main components of the cytoskeleton (microtubules, microfilaments, and intermediate filaments) (Sonnenberg and Liem, 2007; Folli et al., 1994). These studies demonstrate that plectin-1 is an excellent molecular target for pancreatic cancer imaging. In this study, we designed a dual-functional probe which could be detected by optical imaging and MRI. In addition, we showed that the targeted probe was successfully applied in *in vitro* imaging of pancreatic cancer cells and *in vivo* imaging of pancreatic tumor xenografts. Our data provide further supporting evidence that plectin-1 could serve as a molecular target in pancreatic cancer detection.

Most previous studies on pancreatic cancer imaging have used plectin-1 targeted peptide as the target (Bausch et al., 2011; Kelly et al., 2008; Konkalmatt et al., 2013). A recent study successfully used plectin-1 mAb in the synthesis of optomagnetic SPIONs for targeted imaging of pancreatic cancer cells (Wang et al., 2016). Our data are consistent with the report that Plectin-SPION-Cy7 probe was easy to create, stable, and has excellent targeting capability. Magnetic nanoparticles have shown a great promise in malignant tumor imaging and therapy (Wankhede et al., 2012). The nanoparticles can be conjugated with molecules, such as peptides, antibodies, or ligands to create the targeted probe. The characteristics of the targeted probe determined the biological distribution of nanoparticles. Usually, the SPIONs were modified with surfactant, such as PEG to prolong the blood circulation time (Pernia Leal et al., 2015) [32]. PEG also inhibits the separation of NIRF

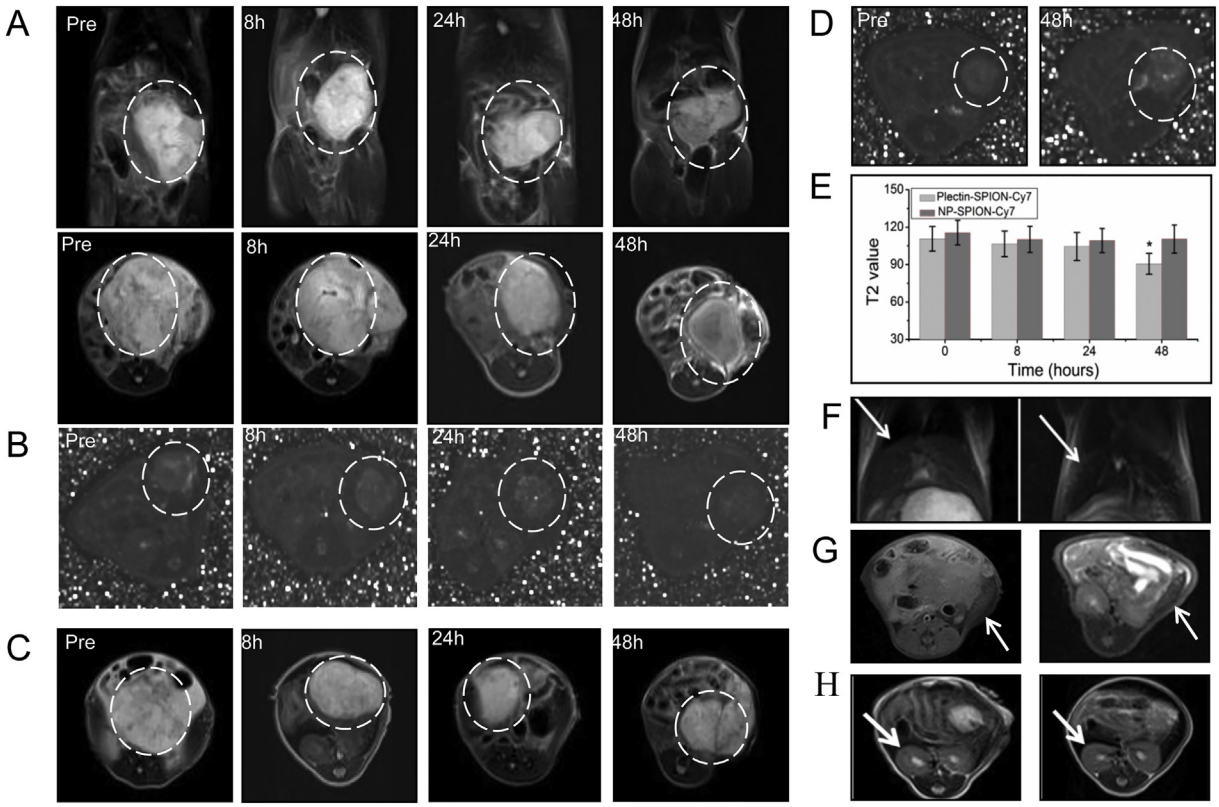

Fig. 6. MR imaging (MRI) of tumor-bearing mice injected with Plectin-SPION-Cy7 or SPION-Cy7. (A) Coronal (upper) and axial (lower) MRI images of mice received Plectin-SPION-Cy7. A T_2 signal reduction is found in tumor area 48 h after administration of the probe through tail vein. (B) Significant reduction of T_2 values in postcontrast tumors (at 48 h) compared with precontrast tumor. (C) No obvious MRI signal changes in mice injected with SPION-Cy7. (D) No reduction of T_2 values in postcontrast tumor (48 h) compared with precontrast tumor. (E) Significantly lower T_2 Values in postcontrast (48 h) *versus* precontrast images (*, $p < 0.001$) and at 48 h *versus* at 8 h and 24 h in mice received Plectin-SPION-Cy7 (*, $p < 0.01$) ($n = 4$) but not in those received SPION-Cy7 ($n = 4$). (F) Reduced signal in the liver (white long arrow) of mice post-injection with the Plectin-SPION-Cy7 (right panel) compared with the pre-injection images (left panel). (G) Reduced signal in the spleen (white arrow) of mice post-injection with the Plectin-SPION-Cy7 (right panel) compared with the pre-injection images (left panel). (H) No obvious signal change is observed in the kidney (white short arrow) of mice post-injection with the Plectin-SPION-Cy7 (right panel) compared with the pre-injection images (left panel).

dyes from the probe. The hydrodynamic size is one of the important characteristics of targeted nanoparticles. Nanoparticles with a hydrodynamic size between 10 and 100 nm have a prolonged blood-circulation time and are small enough to cross the leaky vasculatures inside tumors (Gupta and Wells, 2004). In addition, nanoparticles of these sizes can escape uptake by the liver and easily reach to the target cells (Longmire et al., 2008; Wong et al., 2012). In the present study, the hydrodynamic size of the targeted nanoparticles was 84.35 nm, which allows them to pass through the leaky vasculatures inside tumors and reach the target tumor cells. The potentials of nanoparticles are related to their clearance by Kupffer cells in reticuloendothelial system and to the non-specific binding of cells (Chao et al., 2013). Nanoparticles without optimal potentials are not suitable for *in vivo* imaging. The potentials of our SPION, NP-SPION-Cy7, and Plectin-SPION-Cy7 were 15.9 mV, −24.8 mV, and −11.3 mV, respectively, which are suitable for *in vivo* application. The pharmacokinetic study also showed that the clearance of Plectin-SPION-Cy7 was lower and half-life time was longer than those of NP-SPION-Cy7. The modification with anti-plectin-1 antibody also prolong the blood circulation time. In addition, the potential differences between these three types of nanoparticles indicate the successful binding of plectin-1 antibody and/or Cy7 with the SPION. The magnetic properties and stability of our nanoparticles are acceptable.

Among the many molecular imaging approaches, such as optical imaging (fluorescence and bioluminescence), MR imaging, ultrasound and positron emission tomography, the first two are the most widely used. Fluorescent imaging usually has a high sensitivity, but it could not display the anatomical information and has a very limited tissue penetration depth (Key et al., 2012). MR imaging has relatively low sensitivity, but it could provide the anatomical information together with a high spatial resolution (Taylor et al., 2012). Multi-modality imaging approaches have been used in some studies (Key et al., 2012; Yang et al., 2009). In our study, RFP-expressing XPA-1 cells were used to establish the pancreatic cancer model. Therefore, the tumor could be directly visualized using specific instruments based on red fluorescence, while the NIRF was also detected. Overlapping of the two types of fluorescence indicates the presence of the targeted probes. Optical imaging used in our study also allowed non-invasive whole body imaging of the live experimental animals. Moreover, our targeted probes contains SPION which can shorten T2 and T2*relaxation times, resulting in a signal decrease in MR (Shen et al., 2010). The MR imaging further confirmed that the targeted probes were truly present in the tumor. Thus, the optical and MR imaging are complementary to each other and the multi-modality imaging approaches can cross validate each other.

Although the MR T2 signal was obviously decreased in the liver of mice administered with nanoparticles, Prussian blue staining detected very few iron-positive cells. This could be explained by the blood-rich nature of the liver/spleen and the distribution of the MNPs in the blood. For histological analysis, most of the blood was lost in the tissues sections (<5 μm thickness). Therefore, the nanoparticles in blood could not be observed in histological analysis. Only MNPs that accumulated in

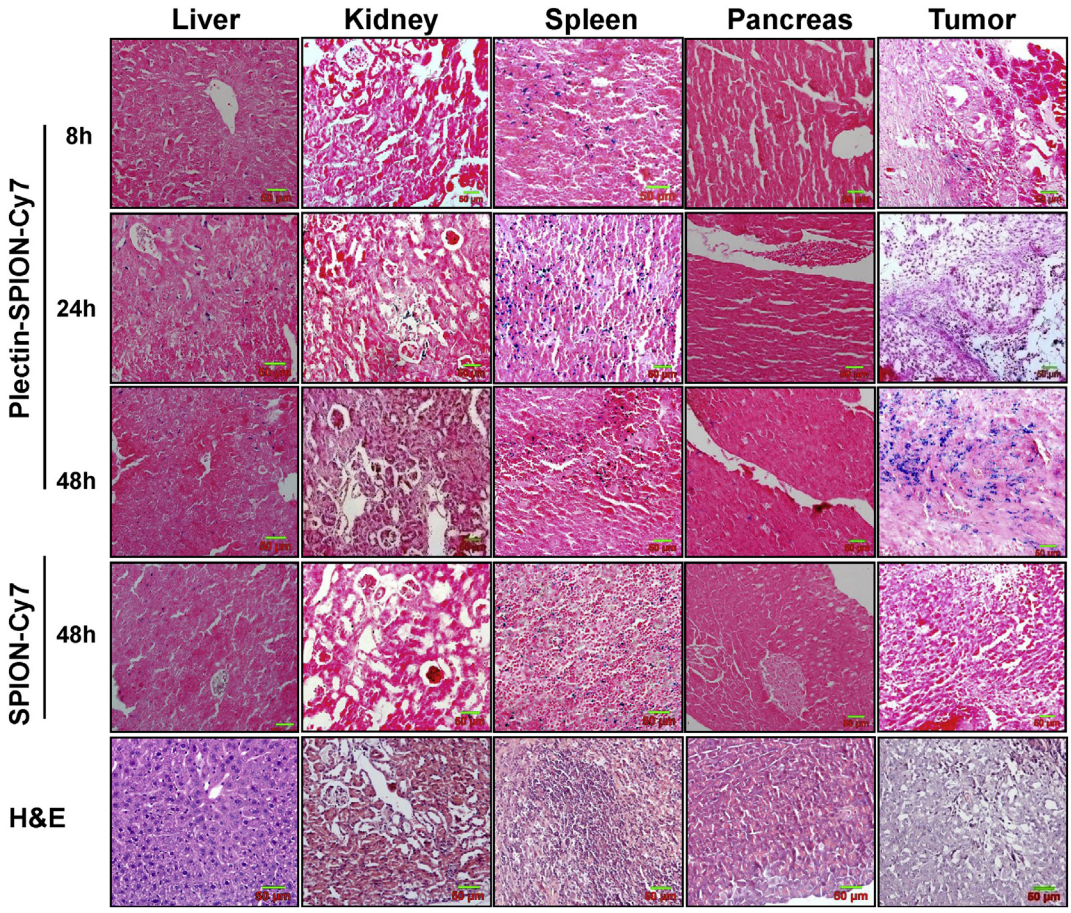

Fig. 7. Hematoxylin and eosin (H&E) and Prussian blue staining of the liver, spleen, kidney, normal pancreatic tissues and pancreatic tumor tissues at 8 h, 24 h and 48 h after the injection of Plectin-SPION-Cy7. A few blue iron particles are found in the liver and tumor tissues at 8 h, 24 h, and much more in the tumor tissues at 48 h. A high number of blue iron particles is found in the spleen at 24 h but was decreased at 48 h. For mice received SPION-Cy7, iron-positive cells are observed in the liver and spleen but very few iron-positive cells were found in the kidney and in the tumors at 48 h.

the Kupffer cells were visible in the liver, in particular at 24 h. In addition, a great number of iron-positive cells were observed in the spleen at 24 h and the number decreased at 48 h, which may suggest a non-specific iron accumulation in the spleen.

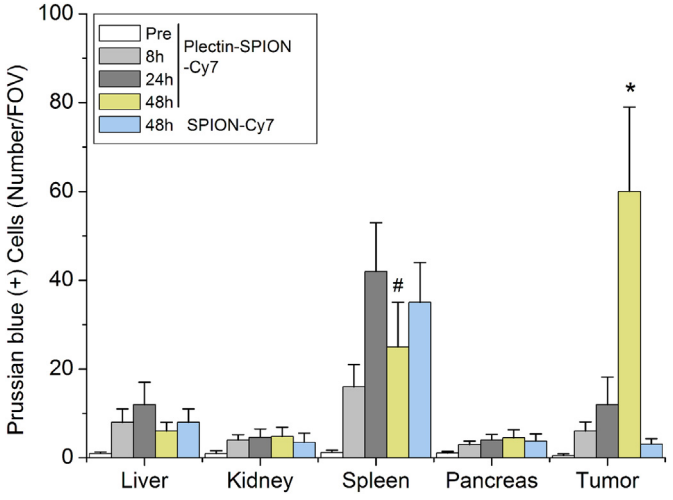

Fig. 8. Prussian blue (+) cells in the normal and cancer tissues. Quantitative data show that Prussian blue (+) cells are mainly distributed in spleen and tumor after administrated with Plectin-SPION-Cy7 or SPION-Cy7 at 8 h, 24 h and 48 h. Prussian blue (+) cells are significantly increased in tumor of mice received Plectin-SPION-Cy7 for 48 h. The number of Prussian blue (+) cells in tumors of mice administrated with Plectin-SPION-Cy7 is significantly higher compared with SPION-Cy7 at 48 h ($p < 0.001$). *$p < 0.01$ *vs* SPION-Cy7; #$p < 0.05$ *vs* 24 h.

There were several limitations in our study. For example, the Cy7 labeled Plectin-SPION could be detected in tumor tissue sections under fluorescence microscopy but we did not conduct such analysis. Second, the size of the xenograft tumors reached to 5 to 10 mm, and it is not clear whether our targeted nanoparticles are suitable for the detection of earlier lesions, such as PanIns I-III. Third, we did not determine the Fe content in cells or tissues using quantitative methods, such as inductively coupled plasma mass spectrometry. Moreover, tissue volume may limit the NIR imaging approach in humans. A probe with an isotopic tracer, such as ^{99}mTc, ^{68}Ga or ^{18}F may be more feasible for clinical applications. We are now exploring the feasibility of linking our probe with isotopic tracers.

In conclusion, we designed a dual-functional plectin-1 targeted nanoparticle probe and showed its preferential accumulation in pancreatic tumors as detected by fluorescent imaging and MRI in a preclinical model. The *in vitro* and *in vivo* imaging results suggest that a plectin-1-targeting molecular probe could be adopted to detect pancreatic cancer.

Conflict of Interests

The authors declare that there are no conflicts of interest.

Author Contributions

Study concept and design: ZQW, XC; acquisition of data: XC, HZ, XSL, ND, YKL, YY, LNS; Analysis and interpretation: ZQW, XC, HZ, SYH, YFZ,

DHL; drafting of the manuscript: XC, HZ, ZQW; critical revision of the manuscript: DHL, ZQW; obtained funding: ZQW.

Acknowledgement

This study was supported by the National Natural Science Foundation of China grants (no. 81471705, 30870689, and 81271630) and Primary Research & Development Plan of Jiangsu Province (BE2017772). The funders did not have any role in study design, data collection, data analysis, interpretation, and writing of the report.

Appendix A. Supplementary data

Supplementary data to this article can be found online at https://doi.org/10.1016/j.ebiom.2018.03.008.

References

Bausch, D., Thomas, S., Mino-Kenudson, M., Fernández-del, C.C., Bauer, T.W., Williams, M., Warshaw, A.L., Thayer, S.P., Kelly, K.A., 2011. Plectin-1 as a novel biomarker for pancreatic cancer. Clin. Cancer Res. 17, 302–309.

Bergmann, U., Funatomi, H., Yokoyama, M., Beger, H.G., Korc, M., 1995. Insulin-like growth factor I overexpression in human pancreatic cancer: evidence for autocrine and paracrine roles. Cancer Res. 55, 2007–2011.

Bogdanov Jr., A., Mazzanti, M.L., 2011. Molecular magnetic resonance contrast agents for the detection of cancer: past and present. Semin. Oncol. 38 (1), 42–54.

Chao, Y., Karmali, P.P., Mukthavaram, R., Kesari, S., Kouznetsova, V.L., Tsigelny, I.F., Simberg, D., 2013. Direct recognition of superparamagnetic nanocrystals by macrophage scavenger receptor SR-AI. ACS Nano 7, 4289–4298.

Chen, Y., Zheng, B., Robbins, D.H., Lewin, D.N., Mikhitarian, K., Graham, A., Rumpp, L., Glenn, T., Gillanders, W.E., Cole, D.J., Lu, X., Hoffman, B.J., Mitas, M., 2007. Accurate discrimination of pancreatic ductal adenocarcinoma and chronic pancreatitis using multimarker expression data and samples obtained by minimally invasive fine needle aspiration. Int. J. Cancer 120, 1511–1517.

Cote, G.A., Smith, J., Sherman, S., Kelly, K., 2013. Technologies for imaging the normal and diseased pancreas. Gastroenterology 144, 1262–1271 (e1).

England, C.G., Kamkaew, A., Im, H.J., Valdovinos, H.F., Sun, H., Hernandez, R., Cho, S.Y., Dunphy, E.J., Lee, D.S., Barnhart, T.E., Cai, W., 2016. ImmunoPET imaging of insulin-like growth factor 1 receptor in a subcutaneous mouse model of pancreatic cancer. Mol. Pharm. 13, 1958–1966.

Folli, S., Westermann, P., Braichotte, D., Pèlegrin, A., Wagnières, G., van den Bergh, H., Mach, J.P., 1994. Antibody-indocyanin conjugates for immunophotodetection of human squamous cell carcinoma in nude mice. Cancer Res. 54, 2643–2649.

Foygel, K., Wang, H., Machtaler, S., Lutz, A.M., Chen, R., Pysz, M., Lowe, A.W., Tian, L., Carrigan, T., Brentnall, T.A., Willmann, J.K., 2013. Detection of pancreatic ductal adenocarcinoma in mice by ultrasound imaging of thymocyte differentiation antigen 1. Gastroenterology 145, 885–894 (e3).

Gupta, A.K., Wells, S., 2004. Surface-modified superparamagnetic nanoparticles for drug delivery: preparation, characterization, and cytotoxicity studies. IEEE Trans. Nanobiosci. 3 (1), 66–73.

Houghton, J.L., Zeglis, B.M., Abdel-Atti, D., Aggeler, R., Sawada, R., Agnew, B.J., Scholz, W. W., Lewis, J.S., 2015. Site-specifically labeled CA19.9-targeted immunoconjugates for the PET, NIRF, and multimodal PET/NIRF imaging of pancreatic cancer. Proc. Natl. Acad. Sci. U. S. A. 112, 15850–15855.

Jemal, A., Siegel, R., Ward, E., Hao, Y., Xu, J., Murray, T., Thun, M.J., 2008. Cancer statistics, 2008. CA Cancer J. Clin. 58, 71–96.

Kelly, K.A., Bardeesy, N., Anbazhagan, R., Gurumurthy, S., Berger, J., Alencar, H., Depinho, R. A., Mahmood, U., Weissleder, R., 2008. Targeted nanoparticles for imaging incipient pancreatic ductal adenocarcinoma. PLoS Med. 5, e85.

Key, J., Knapp, D.W., Leary, J.F., 2012. Multimodal in vivo MRI and NIRF imaging of bladder tumor using peptide conjugated glycol chitosan nanoparticles. Proc. SPIE 8225, 58–69.

Konkalmatt, P.R., Deng, D., Thomas, S., Wu, M.T., Logsdon, C.D., French, B.A., Kelly, K.A., 2013. Plectin-1 targeted AAV vector for the molecular imaging of pancreatic cancer. Front. Oncol. 3, 84.

Lee, M.A., Park, G.S., Lee, H.J., Jung, J.H., Kang, J.H., Hong, Y.S., Lee, K.S., Kim, D.G., Kim, S.N., 2005. Survivin expression and its clinical significance in pancreatic cancer. BMC Cancer 5, 127.

Liu, Z., Liu, H., Ma, T., Sun, X., Shi, J., Jia, B., Sun, Y., Zhan, J., Zhang, H., Zhu, Z., Wang, F., 2014. Integrin alphavbeta(6)-targeted SPECT imaging for pancreatic cancer detection. J. Nucl. Med. 55, 989–994.

Longmire, M., Choyke, P.L., Kobayashi, H., 2008. Clearance properties of nano-sized particles and molecules as imaging agents: considerations and caveats. Nanomedicine (Lond) 3 (5), 703–717.

Massoud, T.F., Gambhir, S.S., 2003. Molecular imaging in living subjects: seeing fundamental biological processes in a new light. Genes Dev. 17, 545–580.

Neesse, A., Hahnenkamp, A., Griesmann, H., Buchholz, M., Hahn, S.A., Maghnouj, A., Fendrich, V., Ring, J., Sipos, B., Tuveson, D.A., Bremer, C., Gress, T.M., Michl, P., 2013. Claudin-4-targeted optical imaging detects pancreatic cancer and its precursor lesions. Gut 62, 1034–1043.

Nichols, L.S., Ashfaq, R., Iacobuzio-Donahue, C.A., 2004. Claudin 4 protein expression in primary and metastatic pancreatic cancer: support for use as a therapeutic target. Am. J. Clin. Pathol. 121 (2), 226–230.

Ntziachristos, V., 2010. Going deeper than microscopy: the optical imaging frontier in biology. Nat. Methods 7, 603–614.

Park, J.Y., Lee, J.Y., Zhang, Y., Hoffman, R.M., Bouvet, M., 2016. Targeting the insulin growth factor-1 receptor with fluorescent antibodies enables high resolution imaging of human pancreatic cancer in orthotopic mouse models. Oncotarget 7, 18262–18268.

Pernia Leal, M., Rivera-Fernandez, S., Franco, J.M., Pozo, D., de la Fuente, J.M., García-Martín, M.L., 2015. Long-circulating PEGylated manganese ferrite nanoparticles for MRI-based molecular imaging. Nanoscale 7, 2050–2059.

Rosenberger, I., Strauss, A., Dobiasch, S., Weis, C., Szanyi, S., Gil-Iceta, L., Alonso, E., González Esparza, M., Gómez-Vallejo, V., Szczupak, B., Plaza-García, S., Mirzaei, S., Israel, L.L., et al., 2015. Targeted diagnostic magnetic nanoparticles for medical imaging of pancreatic cancer. J. Control. Release 214, 76–84.

Shen, Y.M., Yang, X.C., Song, M.L., Qin, C.H., Yang, C., Sun, Y.H., 2010. Growth inhibition induced by short hairpin RNA to silence survivin gene in human pancreatic cancer cells. Hepato-Biliary-Pancreat. Dis. Int. 9, 69–77.

Sonnenberg, A., Liem, R.K., 2007. Plakins in development and disease. Exp. Cell Res. 313, 2189–2203.

Taylor, A., Wilson, K.M., Murray, P., Fernig, D.G., Levy, R., 2012. Long-term tracking of cells using inorganic nanoparticles as contrast agents: are we there yet? Chem. Soc. Rev. 41, 2707–2717.

Tong, M., Xiong, F., Shi, Y., et al., 2013. In vitro study of SPIO-labeled human pancreatic cancer cell line BxPC-3. Contrast Media Mol. Imaging 8, 101–107.

Trajkovic-Arsic, M., Mohajerani, P., Sarantopoulos, A., Kalideris, E., Steiger, K., Esposito, I., Ma, X., Themelis, G., Burton, N., Michalski, C.W., Kleeff, J., Stangl, S., Beer, A.J., et al., 2014. Multimodal molecular imaging of integrin alphavbeta3 for in vivo detection of pancreatic cancer. J. Nucl. Med. 55, 446–451.

Vuong, Q.L., Van Doorslaer, S., Bridot, J.L., Argante, C., Alejandro, G., Hermann, R., Disch, S., Mattea, C., Stapf, S., Gossuin, Y., 2012. Paramagnetic nanoparticles as potential MRI contrast agents: characterization, NMR relaxation, simulations and theory. MAGMA 25, 467–478.

Wang, X., Xing, X., Zhang, B., Liu, F., Cheng, Y., Shi, D., 2014. Surface engineered antifouling optomagnetic SPIONs for bimodal targeted imaging of pancreatic cancer cells. Int. J. Nanomedicine 9, 1601–1615.

Wang, Z., Tong, M., Chen, X., Hu, S., Yang, Z., Zhang, Y., Zhou, H., Wu, Y., Li, X., Li, D., 2016. Survivin-targeted nanoparticles for pancreatic tumor imaging in mouse model. Nanomedicine 12 (6), 1651–1661.

Wankhede, M., Bouras, A., Kaluzova, M., Hadjipanayis, C.G., 2012. Magnetic nanoparticles: an emerging technology for malignant brain tumor imaging and therapy. Expert. Rev. Clin. Pharmacol. 5, 173–186.

Weissleder, R., 2006. Molecular imaging in cancer. Science 312, 1168–1171.

Weissleder, R., Ntziachristos, V., 2003. Shedding light onto live molecular targets. Nat. Med. 9, 123–128.

Willett, C.G., Czito, B.G., Bendell, J.C., Ryan, D.P., 2005. Locally advanced pancreatic cancer. J. Clin. Oncol. 23, 4538–4544.

Wong, R.M., Gilbert, D.A., Liu, K., Louie, A.Y., 2012. Rapid size-controlled synthesis of dextran-coated, 64Cu-doped iron oxide nanoparticles. ACS Nano 6 (4), 3461–3467.

Yang, L., Mao, H., Cao, Z., Wang, Y.A., Peng, X., Wang, X., Sajja, H.K., Wang, L., Duan, H., Ni, C., Staley, C.A., Wood, W.C., Gao, X., et al., 2009. Molecular imaging of pancreatic cancer in an animal model using targeted multifunctional nanoparticles. Gastroenterology 136, 1514–1525 (e2).